

Mechanisms of nanooxidation of Si(100) from atomic force microscopy

Te-Hua Fang*

Department of Mechanical Engineering, Southern Taiwan University of Technology, Tainan 710, Taiwan

Received 22 April 2004; received in revised form 21 June 2004; accepted 30 June 2004

Abstract

The machining characteristics of the nanolithographic process were studied using atomic force microscopy. Nano-oxidation experiments were conducted to investigate the influence that the different experimental parameters had on height, width and the growth rate of the nanowires and nanodots as well as upon the machining efficiency. The experimental parameters included; the applied voltage, humidity, scanning oxidization time, crystalline orientation and the shape of the probe tip. The results indicated that as the oxidization time and the applied voltage were increased, the nanowire's height and width also increased. 'Also, a nanowire with increased height was produced when the humidity was higher. Finally as the probe tip began to wear and the tip's radius increased, a nanowire with a higher height and width was produced.

© 2004 Elsevier Ltd. All rights reserved.

Keywords: Nano-oxidation; Atomic force microscopy; Nanolithography; Silicon; Wear

1. Introduction

Scanning probe microscopy (SPM) has recently attracted much attention for its potential to produce patterns with lateral resolution on a nanometer scale [1]. Nanometer-sized features have been successfully defined using one or more of the processes; exposure of resists [2], decomposition of organometallic compounds [3], selective oxidation of hydrogenated silicon [4], or amorphous silicon [5].

Recently, the formation of oxide layers was produced on titanium film using atomic force microscopy (AFM) [6]. Nano-oxidation can be used to extend the application field of AFM-based lithography, when nano-patterning of the isolated layers is needed in silicon technology. The best candidate clearly appears to be noncontact mode AFM for the generation of oxide patterns on silicon substrate due to the soft interaction between the surface and the tip [7].

There are two advantages in using AFM for lithography. First, the electric field governing the exposure mechanism can be applied independently. Second, noncontact-mode

AFM eliminates lateral shear forces and overcomes the tip-sample adhesion forces and capillarity, thereby avoiding damage to the surface and improving imaging and lithography resolution [6].

In this paper the characteristics of nanoscale oxidation patterns on silicon were investigated by using AFM in a noncontact mode. The dimensional characteristics of the oxide structures were studied as a function of the applied voltage, humidity, crystalline orientation, the tip shape and oxidation time.

2. Experimental details

All the experiments were performed using atomic force microscopy (NT-MDT SPM, Russia) operated in a non-contact mode. A silicon cantilever with a TiN coated probe (30 $\mu\Omega$ cm) was used. The average force constant and the resonance frequency were 34 N/m and 350 kHz, respectively. The cantilever was exercised at its resonance frequency. To perform the oxidation an additional circuit was used to apply a voltage between the tip and the substrate.

* Tel.: +886-6-2533131; fax: +886-6-2425092.
E-mail address: fang@mail.stut.edu.tw.

The samples were p-type Si(100) with a surface resistivity of 20 Ω cm. Due to the surface being exposed to air it had a native-oxide layer of about 2 nm. The AFM apparatus was placed into a sealed clean environment with access to insert dry or H₂O-saturated nitrogen. The relative humidity ranged from 30 to 85%.

The topography feedback was switched off during the nano-lithographic process [8]. The process to nano-oxidize the Si surface using AFM noncontact mode had three important steps [9]: First, an oscillating probe is placed about 10 nm above the sample surface. Second, a voltage pulse is applied to form a liquid bridge between the tip and sample. Third, another voltage is applied to the silicon substrate to induce nano-oxidation.

Anodization by the water on the specimen's surface will occur directly below the AFM probe tip when a negative bias voltage is applied to the probe. In Fig. 1 the AFM local anodic oxidation on a Si (100) surface is shown. There is an adsorbed water layer on the surface, which provides the required electrolyte under ambient conditions. The thickness of the water layer depends on the relative humidity level in the surrounding air. Using the AFM tip as a cathode, the surface of Si (100) will be oxidized, and the ions (including OH⁻ and O²⁻) contribute to the formation of the surface oxide; then the nanooxidized structure will be made.

The occurrence of the oxidation mechanism on the surface of the Si substrate was as follows; First, the silicon surface was de-passivated by replacing the Si-H bonds with Si-OH bonds [10]. Once the surface had been de-passivated, the first layer of Si-Si bonds become polarized due to the high electronegativity of the OH⁻ and then the Si-Si bonds reacted to the polar H₂O molecules to form a monolayer of silicon oxide [11]. Second, the electrical field was created between the first silicon oxide layer and the substrate, which caused the OH⁻ to drift through the oxide film, increasing the oxide film's thickness [12]. Third, in the anodic regime, this dependence was stronger because the electrical field not only enhances OH⁻ formation, but also had the correct direction to cause the OH⁻ diffusion through the oxide film. On the contrary, the effect of the electric field on the cathodic modifications could have only created an enhancement to the OH⁻ formation [13].

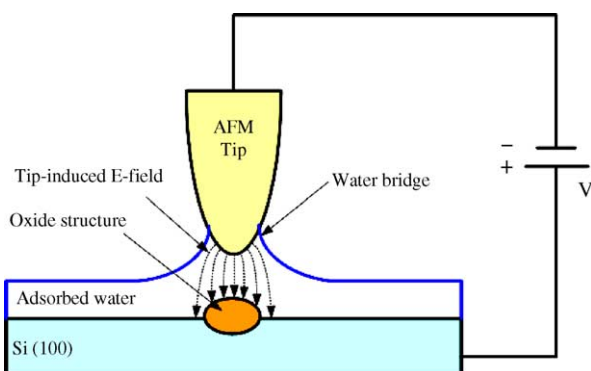


Fig. 1. Schematic of the principle of AFM anodization.

3. Results and discussions

3.1. Effect of parameters on nanowires

Fig. 2(a) shows the size of the oxide nanowires created at the applied voltages of 6, 7, 8, 9 and 10 V. The larger applied voltages induced a larger electric field effect, which caused a stronger interaction to occur between the tip and the surface. Fig. 2(b) shows the height and the width of the oxide nanowire as a function of the anodisation voltage applied to the Si surface.

To understand the influence that humidity had on the size of an oxide nanowire, the probe tip was placed at a fixed distance above the sample's surface at different relative humidity conditions of 48, 55, 74 and 85%. In Fig. 3 it can be seen that as the humidity was increased the size of the oxide nanowires also increased. It can be seen that the lateral and vertical dimensions of the resulting oxide wires have a direct relationship to the amount of induced

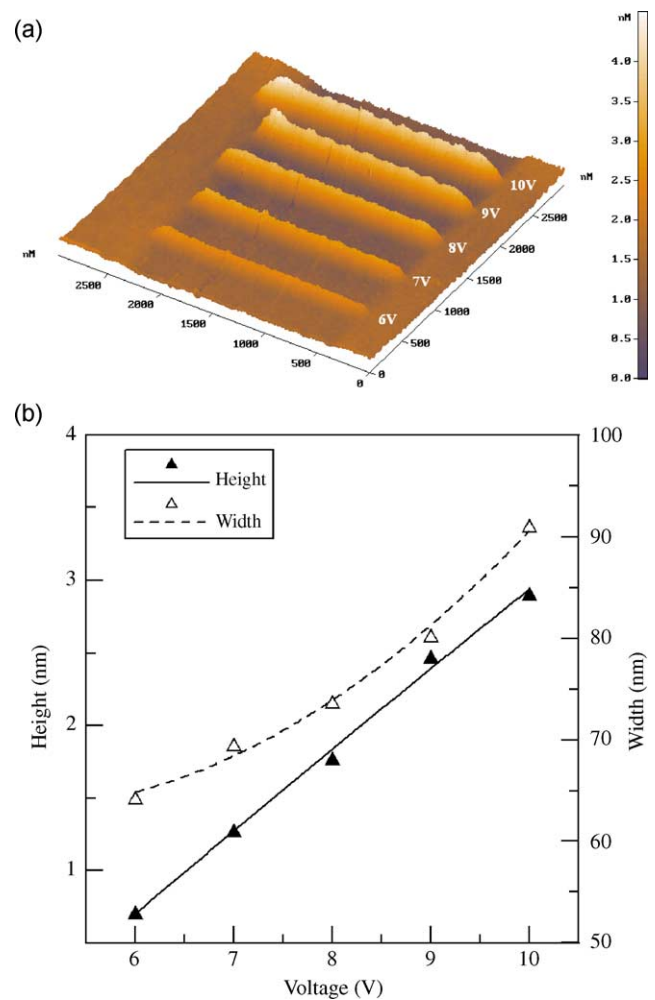


Fig. 2. (a) AFM image showing the nanowires created at the applied voltages of 6,7,8,9 and 10 V. (b) Nanowire's height and width created at different applied voltages.

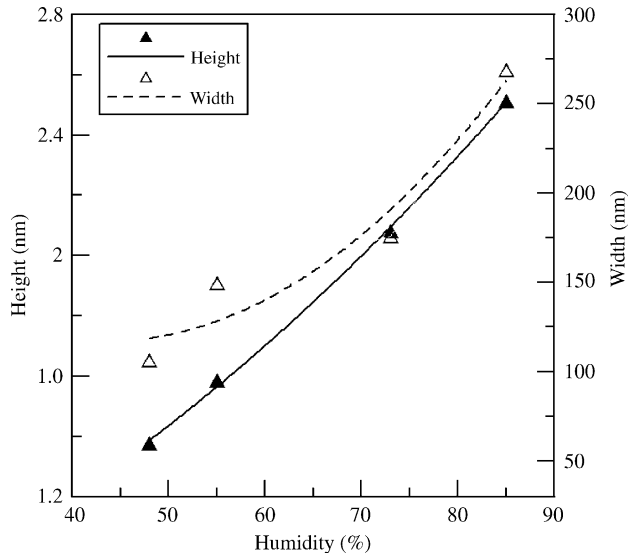


Fig. 3. Nanowire's height and width as related to the relative humidity.

humidity. This is due to the electric field effect initiating the oxide mechanism, as the humidity increased, the electro-chemical interaction between the tip and the surface becomes stronger.

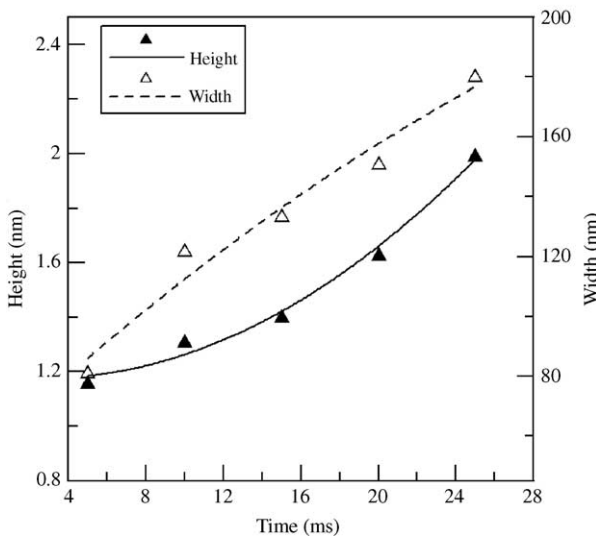
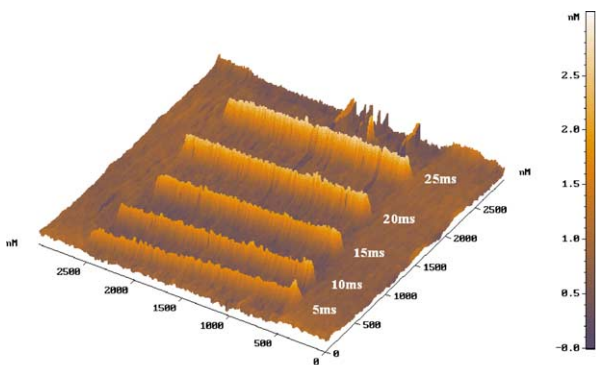


Fig. 4. (a) AFM image showing the nanowires created at the different oxidation times of 5,10,15,20, and 25 ms. (b) Nanowire's height and width created at different oxidation times.

Fig. 4(a) shows the size of the oxide nanowire produced on a silicon film using different oxidation time. The observed relationship of the oxide nanowire height to the probe tip's oxidation time can be explained by the field-assisted oxidation theory of very thin films [6]. Fig. 4(b) shows the height and width of the oxide nanowire produced at different oxidation times. The largest oxide nanowire corresponded to the longest oxidation time. The lateral resolution was determined by the oxide nanowire's width and was found to be proportional to the oxide nanowire's height.

To understand the machining process efficiency, the material growth rate η determined the volume of oxide nanowires produced per second. This was done by taking

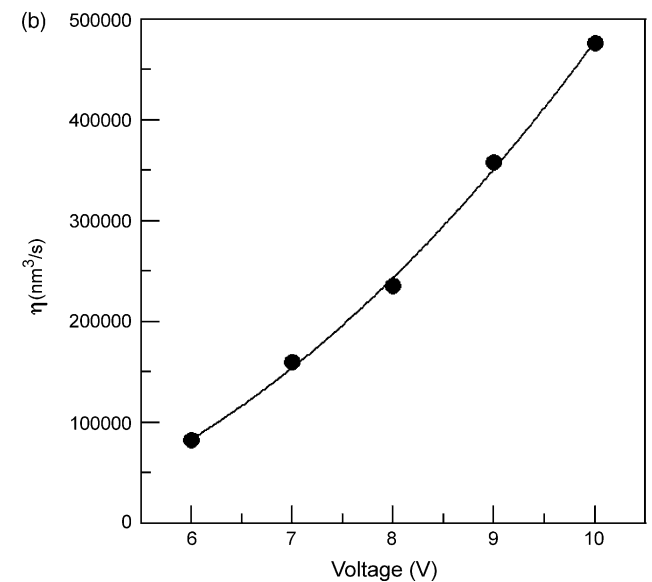
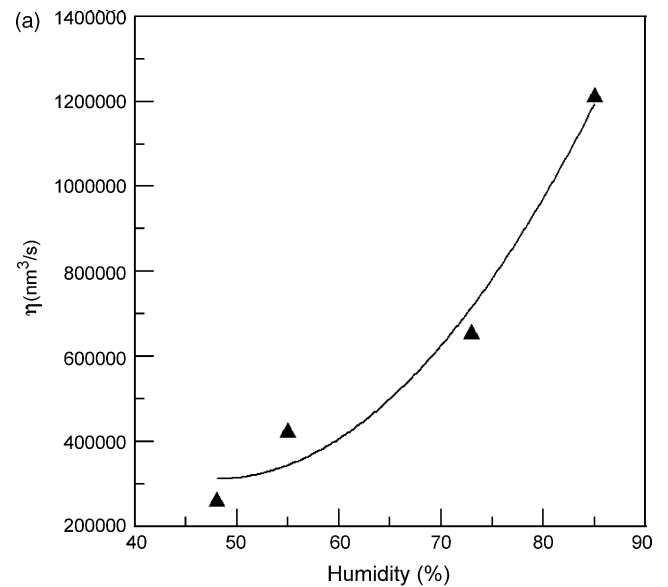


Fig. 5. (a) Material growth rate of the oxidation process under different humidities. (b) Material growth rate of the oxidation process under different applied voltages.

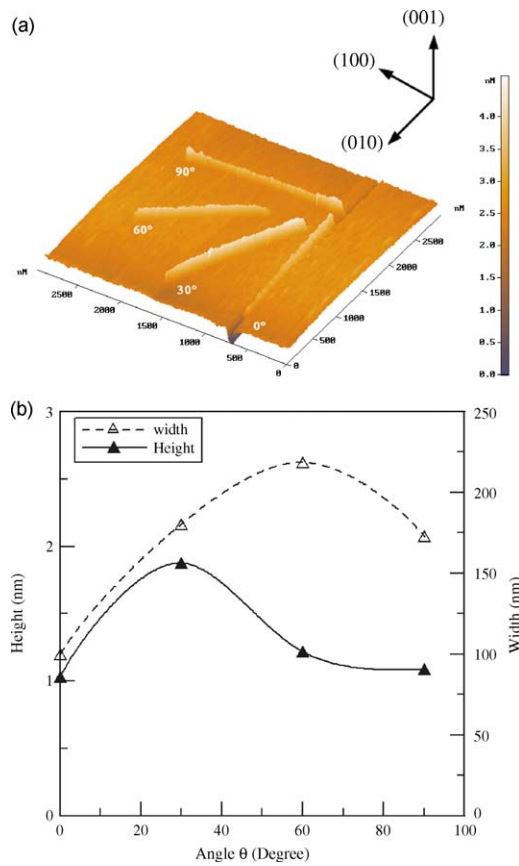


Fig. 6. (a) AFM image showing the nanowires created at different crystalline orientations. (b) Nanowire's height and width at different crystalline orientations.

a cross sectional area of the nanowires taken from three distinct positions and average, then multiplying it by the oxide nanowire's length. The volume of the growth material can be used to evaluate the efficiency of the oxidation process using different operating parameters.

The growth volume rate at different humidity levels and voltages are shown in Fig. 5(a) and (b). The volume increased as the humidity was increased. Similar results were obtained when the voltage was increased at a fixed humidity. These results are consistent with the observations that the base voltage mainly affects the nanowire's height and width.

Fig. 6(a) represents an AFM image of four oxide nanowires at different crystalline orientations. The highest nanowire was obtained at 30° and its dimensions were a width of 170 nm and a height of 1.8 nm. This is one of the smallest dimensions obtained through the use of AFM-based lithography in ambient air. The height and width of the oxide nanowires at different crystalline orientations are shown in Fig. 6(b). The oxide nanowire growth rate was different at each crystalline orientation.

3.2. Effect of parameters on nanodots

Fig. 7 depicts a sequence of AFM imaged oxide dots fabricated using the AFM-based oxidation method. The patterns in Fig. 7 were obtained by using a constant voltage of 10 V at the different oxidation times of 50, 10, 5, 1 and 0.5 s. These experiments were carried out in an environment having 65% relative humidity.

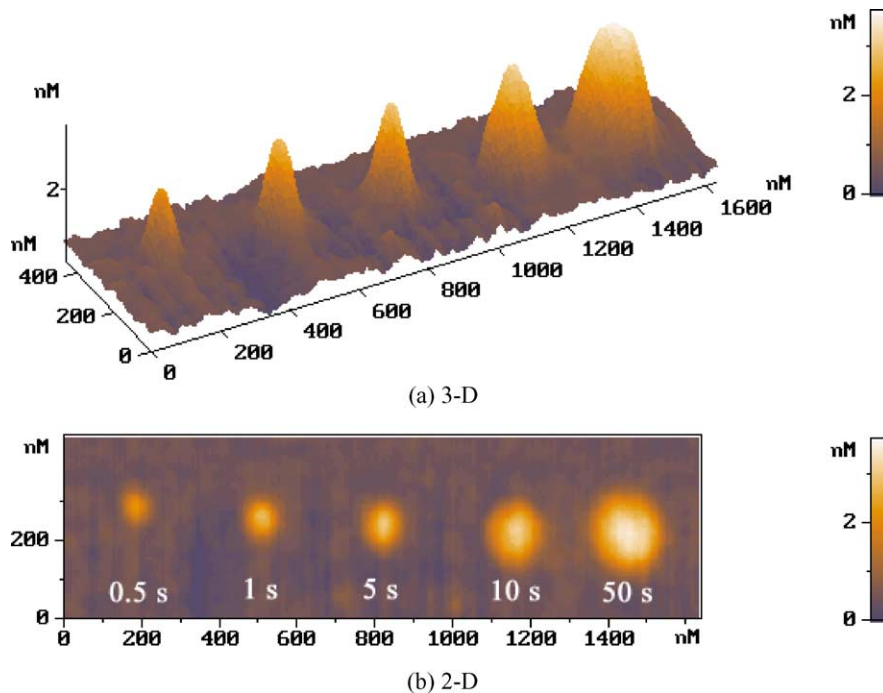


Fig. 7. AFM image showing the nanodots created at the different oxidation times of 0.5, 1, 5, 10, and 50 s.

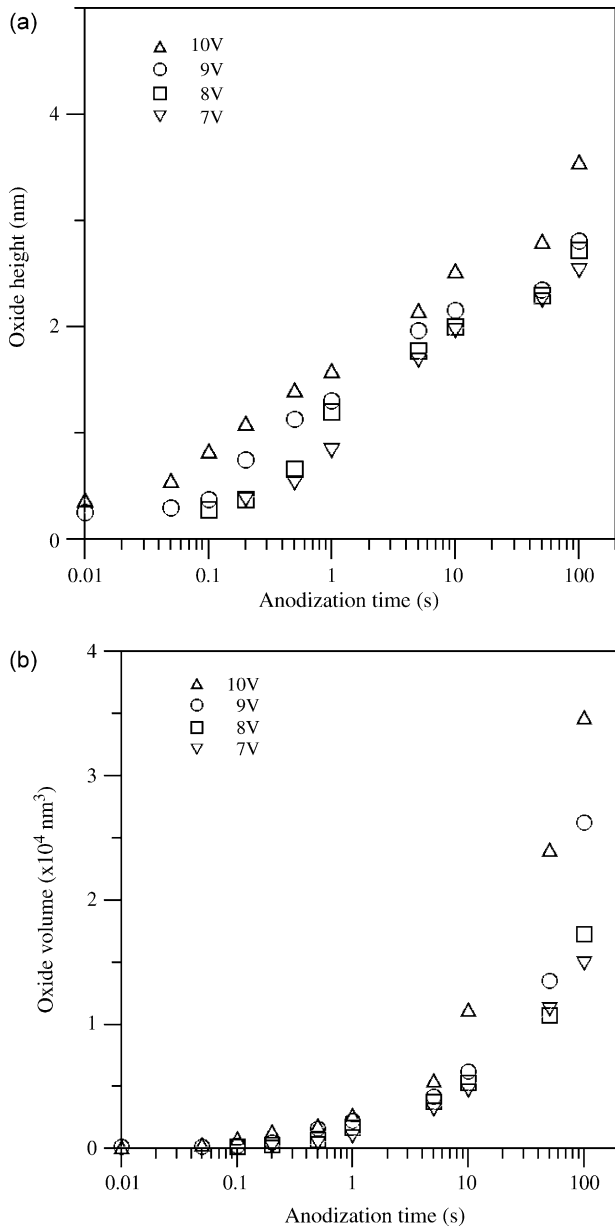


Fig. 8. Oxide height and volume of the oxidation process under different anodization times.

It was found that a longer anodization time and a larger anodization voltage resulted in larger and higher oxidized dots shown in Fig. 8(a) and (b). This implies that the oxide dots not only grow along the vertical direction but also along the horizontal direction. Fig. 8(a) and (b) represent the oxide height and oxide volume as a function of the anodization time at the four anodization voltages. It can be seen that the oxide height and oxide volume increased as the logarithm of the anodization time increased and when the anodization voltage was increased. To fabricate a dot for a given size the anodization times should be shorter or longer in relationship to the corresponding anodization voltages which would be higher or lower, respectively.

This is to say when using a shorter anodization time a higher anodization voltage should be used and when using a longer anodization time a lower anodization voltage should be used to fabricate dots of equal proportion and mechanisms.

The relationships of the growth rate and the electric field strength can be obtained as shown in Fig. 9(a). In Fig. 9(a) it can be seen that the growth rate increased as the electric field strength and applied anodization voltages were increased. The initial growth rate was on the order of $\sim 100 \text{ nm/s}$ at 10 V, it decreased rapidly as the electric field

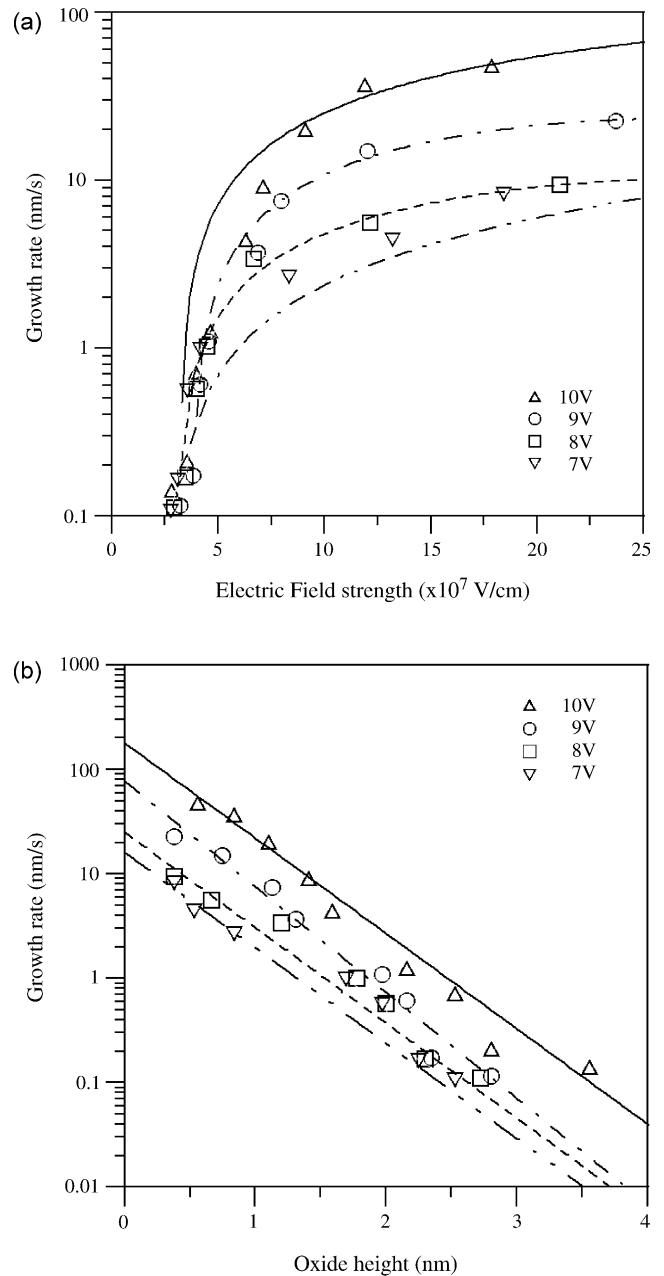
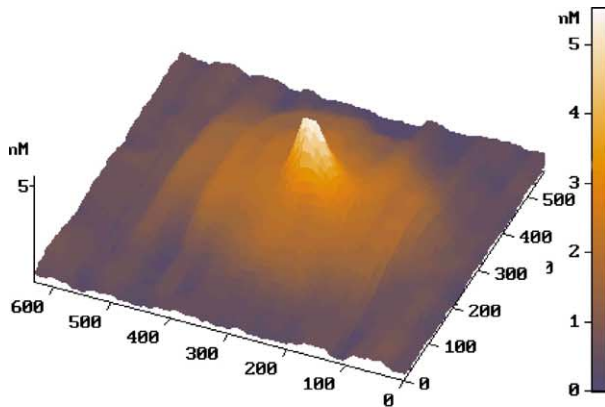
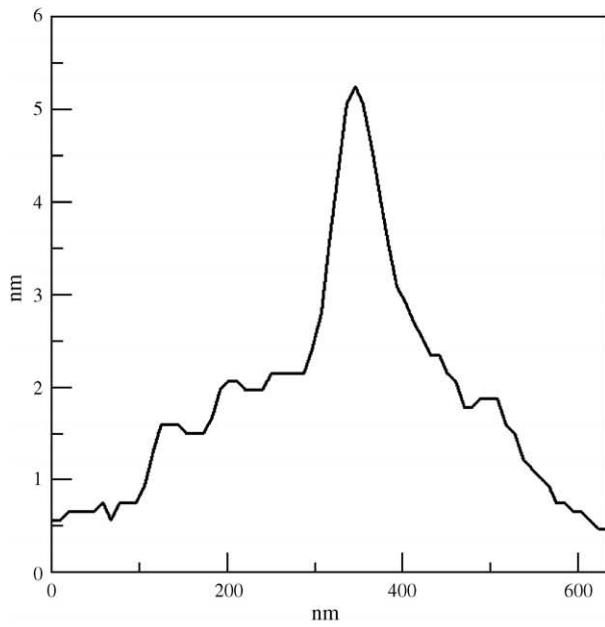
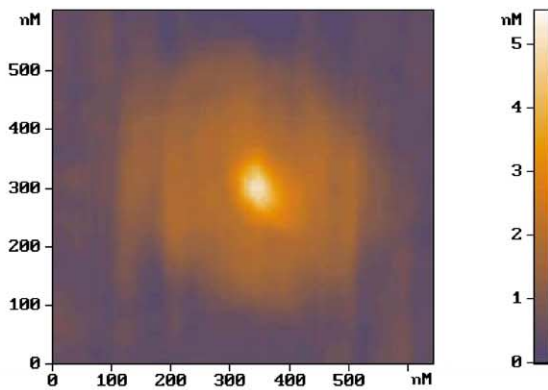


Fig. 9. Growth rate of the oxidation nanodots under different anodization voltages.



(a) 3-D AFM image



(b) 2-D AFM image

Fig. 10. The two-storied shaped dot generated by nano-oxidization of a Si surface.

strength was decreased. In addition to that it was found that the anodization process was enhanced when the electric field strength was at an order of $2\text{--}3 \times 10^7$ V/cm. As pointed out in Avouris et al. [14], an equation was used to describe

the growth kinetics as follows:

$$\frac{dh}{dt} \propto \exp\left(-\frac{h}{l_c}\right) \tag{1}$$

where h is the oxide height at time t , and l_c is a characteristic length depending on the anodization voltage. The relationships between the growth rate and the oxide height at four different applied bias voltages are plotted in Fig. 9(b). In this experiment the growth rate exponentially decreased as the oxide height was increased.

The dot shape was decided under the balance between the ionic diffusion and space charge during the oxidation process. Fig. 10 shows the AFM image of the two-storied shaped dot produced under an applied voltage of 10 V above the relative humidity of 80%. The two-storied shaped dot consisted of the core part and the base part. The core part was made under the probe tip and it increased in size, compared with the continuous lateral spread of the base part.

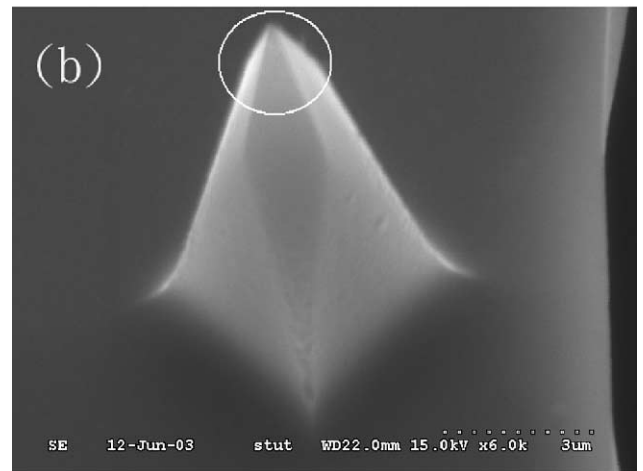
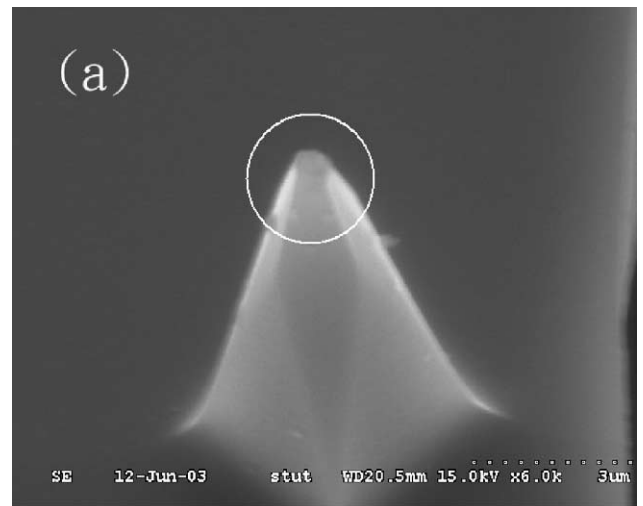


Fig. 11. (a) An AFM tip with a larger radius due to wear after oxidation time of 10 h. (b) SEM image of AFM tip use to perform the oxidation experiments.

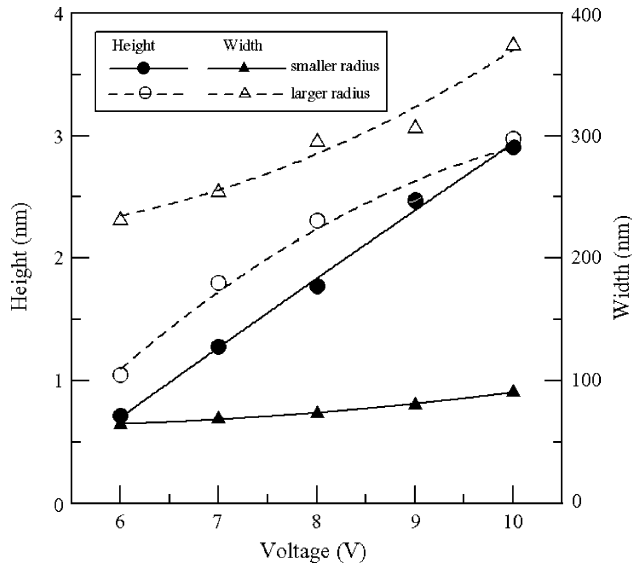


Fig. 12. Nanowire's height and width using different tip radii.

The base part was made by the diffusing ion current. The contribution of ion diffusion under different relative humidity was discussed in Kuramochi et al. study [15]. They suspected that the increasing of the dot volume for a long oxidation time was due to the ionic diffusion.

3.3. Wear of AFM probe tip

The wear behavior of the AFM probe tip was taken into consideration when the probe tip was used for the nano-oxidation process. Fig. 11(a) and (b) show the SEM images of a typical AFM tip radius and an AFM probe tip radius after 10 continuous hours of nano-oxidation processing.

As the probe tip use was increased the tips radius became larger, which produced a larger reactive area between the sample surface and the tip. Higher and wider oxide nanowires were formed as shown in Fig. 12 using a worn AFM probe with a larger tip radius.

4. Conclusions

In this paper, nano-oxidation experiments were carried out to study the characteristics of the AFM-based lithography process as a basis for the future development of nanomachining tools. From this study, several important conclusions were reached as follows:

- (1) The applied voltage and the humidity were related to the oxide nanowires height and width. As the applied voltage and the humidity were increased the oxide nanowire's height and width increased.
- (2) The machining efficiency, as determined by material growth rate, was mainly affected by the applied voltage and humidity.
- (3) The anodization process was enhanced when the electric field strength was at an order of $2\text{--}3 \times 10^7$ V/cm. The growth rate decreased which would be attributed to reduction of the electric field strength when the oxide height increased.
- (4) Above a relative humidity of 80% a two-storied shaped nanodot caused by the ionic diffusion was found.
- (5) As the tip radius was enlarged through continuous use and the oxidation time was increased, the oxide nanowire's height and width increased.

Acknowledgements

The author would like to thank Shi-Cheng Liao for technical assistance and this work was partially supported by the National Science Council of Taiwan, under Grant No. NSC92-2218-E218-006.

References

- [1] T.H. Fang, C.I. Weng, J.G. Chang, *Nanotechnology* 11 (2000) 181.
- [2] A. Majumdar, P.I. Oden, J.P. Carrejo, L.A. Nagahara, J.J. Graham, J. Alexander, *Appl. Phys. Lett.* 61 (1992) 2293.
- [3] M.A. McCord, D.P. Kern, T. Chang, *J. Vac. Sci. Technol. B* 6 (1988) 1877.
- [4] J.A. Dagata, J. Schneir, H. Harary, C. Evans, M. Postek, J. Bennett, *Appl. Phys. Lett.* 56 (2001) 1990.
- [5] N. Kramer, J. Jorritsma, H. Birk, C. Schonenberger, *J. Vac. Sci. Technol. B* 13 (1995) 805.
- [6] E. Dubois, J.L. Bubbendorff, *Solid-State Electron.* 43 (1999) 1085.
- [7] E.S. Snow, P.M. Campbell, *Appl. Phys. Lett.* 64 (1994) 1932.
- [8] M. Calleja, R. García, *Appl. Phys. Lett.* 76 (2000) 3427.
- [9] D. Wang, L. Tsau, K.L. Wang, *Appl. Phys. Lett.* 65 (1994) 1415.
- [10] C. Schonenberger, N. Kramer, *Microelectron. Eng.* 32 (1996) 203.
- [11] A.E. Gordon, R.T. Fayfield, D.D. Litfin, T.K. Higman, *J. Vac. Sci. Technol. B* 13 (1995) 2805.
- [12] S.L. Yau, F.F. Fan, A.J. Bard, *J. Electrochem. Soc.* 139 (1992) 2825.
- [13] G. Abadal, F. Perez-Murano, N. Barinol, X. Aymerich, *Appl. Phys. A* 66 (1998) S791.
- [14] P. Avouris, T. Hertel, R. Martel, *Appl. Phys. Lett.* 71 (1997) 285.
- [15] H. Kuramochi, K. Ando, H. Yokoyama, *Surf. Sci.* 542 (2003) 56.